ELSEVIER

Sedimentary Geology 120 (1998) 55–74

Sedimentary Geology

Precambrian tidal and glacial clastic deposits: implications for Precambrian Earth–Moon dynamics and palaeoclimate

George E. Williams *

Department of Geology and Geophysics, University of Adelaide, Adelaide, SA 5005, Australia

Received 28 February 1997; accepted 13 June 1997

Abstract

Over the past decade the study of Precambrian clastic tidal rhythmites — stacked laminae of sandstone, siltstone and mudstone that display periodic variations in thickness reflecting a strong tidal influence on sedimentation — has provided accurate palaeotidal and palaeorotational data. Palaeotidal records obtained from tidal rhythmites may be systematically abbreviated, however, and derived periods and frequencies can be misleading. The validity of such values, including past length of day, can be assessed by testing for internal self-consistency through application of the laws of celestial mechanics. Such a test supports the estimated length of day of 21.9 ± 0.4 h derived from the late Neoproterozoic (~620 Ma) Elatina–Reynella rhythmites in South Australia, and the indicated mean rate of lunar retreat of 2.16 ± 0.31 cm/year since ~620 Ma. The validity of estimated lengths of day obtained from other Precambrian tidal rhythmites remain unverified because the data sets contain only one primary value directly determined from the rhythmites. The Elatina–Reynella data militate against significant Earth expansion at least since ~620 Ma, and suggest that the free nutation or 'tipping' of the Earth's fluid core has undergone a resonance with the Earth's annual forced nutation since the Neoproterozoic. Glaciogenic deposits are readily distinguishable from ejecta resulting from impacts with Earth-crossing bodies. Palaeomagnetic data, based on the geocentric axial dipole model for the geomagnetic field, indicate that Neoproterozoic and Palaeoproterozoic glaciation and cold climate near sea level occurred in low palaeolatitudes. This enigmatic finding may imply global glaciation or an increased obliquity of the ecliptic, and is relevant to modelling the effect of ice sheet formation on the Earth's obliquity history by obliquity–oblateness feedback mechanisms. Through multidisciplinary studies, clastic sedimentology and geophysics together can make substantial contributions to understanding Precambrian Earth–Moon dynamics and global palaeoenvironments.

Keywords: Precambrian; tidal environment; Earth–Moon system; glacial deposits; palaeomagnetism; palaeoclimate

1. Introduction

Clastic sedimentologists, by pursuing palaeogeophysical implications of their research, can contribute to understanding Precambrian Earth–Moon dynamics and palaeoenvironments.

Over the past decade, the study of Precambrian clastic tidal rhythmites has provided quantitative palaeogeophysical information, including the Precambrian length of day and Earth–Moon distance and a test of Earth expansion. This paper reviews such research, emphasises the potential pitfalls in analysing tidal rhythmite measurements, and assesses the geophysical validity of determined Precambrian palaeotidal and palaeorotational periods

* Tel.: +61 (8) 8303-5843; Fax: +61 (8) 8303-4347; E-mail: gwilliams@geology.adelaide.edu.au

0037-0738/98/$ – see front matter
PII S0037-0738(98)00027-X

and frequencies. Milankovitch orbital cycles are not discussed because quantitative analysis of such cycles in the Precambrian stratigraphic record has barely begun, but with a smaller Precambrian Earth–Moon distance the periods of the precession and obliquity cycles will be shorter than those of the Phanerozoic.

A feature of Precambrian stratigraphy is the episodic development of widespread glaciogenic successions in the Neoproterozoic and Palaeoproterozoic. Compilations on glacial geology (Hambrey and Harland, 1981; Eyles, 1993; Deynoux et al., 1994) show that the great majority of interpretations of glacial deposition are valid and, as discussed here, recent claims that many diamictites previously interpreted as tillites are impact ejecta (e.g. Oberbeck et al., 1993) cannot be sustained. A more interesting debate, which has run for nearly four decades, is whether Neoproterozoic ice sheets formed near sea level in low palaeolatitudes. As reviewed here, recent palaeomagnetic research on both Neoproterozoic and Palaeoproterozoic glaciogenic rocks has indeed revealed the Precambrian climatic paradox of palaeoequatorial glaciation and cold climate near sea level. This enigmatic finding has generated lively and on-going debate as to the possible causes of low-palaeolatitude glaciation.

2. Clastic tidal rhythmites

2.1. Importance to tidal sedimentology and palaeogeophysics

Tracing the history of the Earth's deceleration and the Moon's retreat under the influence of tidal friction, whereby angular momentum is transferred from the Earth's rotation to the Moon's orbital motion, is a major challenge for Earth scientists. The implications of backward extrapolation of the present rate of lunar retreat are catastrophic: between 1500 and 2000 Ma, tidal forces would have disrupted the Moon or caused the total melting of the Earth's mantle and the Moon (Lambeck, 1980). No evidence exists for such events at that time and growth patterns of stromatolites indicate the presence of lunar tides at 3000 Ma (Pannella, 1976).

Hopes that the latter history of the Earth's rotation and the Moon's orbit could be accurately traced from the study of skeletal growth increments in marine invertebrate fossils (Rosenberg and Runcorn, 1975) have not been fully realised. The Palaeozoic data, if taken at face value, imply little overall change in tidal friction over the past 500 m.y. and thus do not avert a catastrophic close approach of the Moon at about 2000 Ma. Lambeck (1980) questioned the validity of much of the Palaeozoic data and Scrutton (1978) concluded that the values obtained from fossils "should be treated as approximations rather than as precise quantities for mathematical analysis". Furthermore, the reliability of palaeorotational data based on stromatolite growth patterns is unclear. Because of such difficulties, little new work has been done on palaeontological 'clocks' since the 1970s.

Over the past decade, the study of clastic tidal rhythmites — vertically accreted laminae of fine-grained sandstone, siltstone and mudstone that display periodic variations in thickness reflecting a strong tidal influence on sedimentation (Fig. 1) — has rejuvenated palaeogeophysical analysis of the Earth–Moon system and extended such study into the Precambrian. Tidal rhythmites have been described from the Neoproterozoic (Williams, 1989a,b,c, 1991; Deynoux et al., 1993; Chan et al., 1994) and also from Phanerozoic and modern deposits (see Smith et al., 1991). Inferred palaeoenvironments range from estuarine to upper and lower delta slope and distal ebb-tidal delta. The ebb-tidal setting (Fig. 2) may be optimum for the deposition of tidal rhythmites: it is envisaged that fine-grained sediment is entrained by ebb-tidal currents in a tidal inlet and transported mainly in suspension by strong ebb-tidal currents, plumes or jets (Özsoy, 1986) to deeper water offshore, where the suspended sediment settles to form graded laminae. Periodic changes in lamina thickness reflect variations in the amount of sandy and silty material entrained and deposited by tidal currents in response to periodic changes in the height, speed and range of tides. Such rhythmites would represent the more distal complement of the well known cross-bedded tidal 'bundle' facies. The preservation potential of Precambrian tidal rhythmites, particularly finely laminated distal deposits, may be enhanced by the lack of bioturbation by benthic fauna in Precambrian times.

The development of tidal estuaries and inlets that are suitable for the deposition of tidal rhythmites

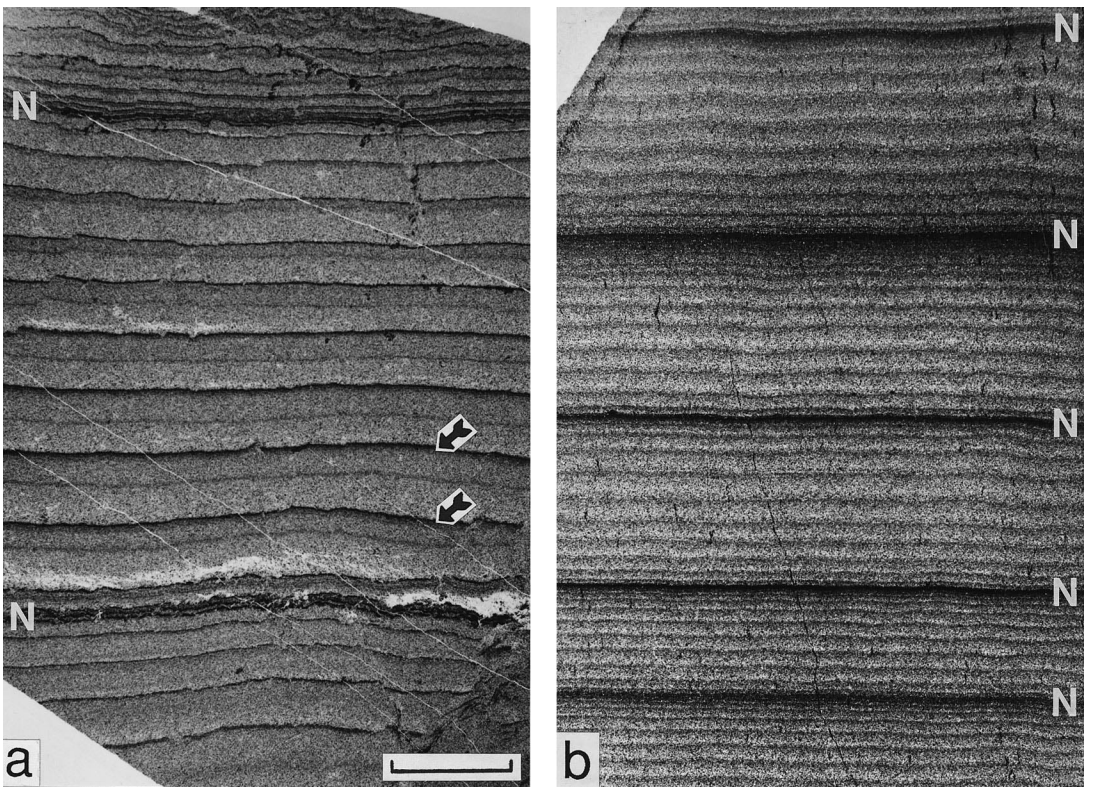

Fig. 1. Late Neoproterozoic (~620 Ma) tidal rhythmites, South Australia. Mudstone bands appear darker than sandy to silty laminae. *N* marks positions of neap-tidal bands. Scale bar 1 cm, for both photographs. (a) Reynella Siltstone, showing one thick, fortnightly neap–spring cycle that contains about 14 diurnal (lunar day) laminae of fine-grained sandstone; the thicker diurnal laminae have mudstone tops (arrows) and comprise two semidiurnal sublaminae. (b) Elatina Formation. Four fortnightly neap–spring cycles, each comprising between 10 and 14 graded diurnal laminae of very fine-grained sandstone and siltstone, are bounded by thin mudstone bands deposited at neap tides.

may be favoured by glacio-eustatic rise of sea level. Modern examples of such settings where tidal rhythmites are accumulating include Glacier Bay, Alaska (Smith et al., 1990) and the Bay of Fundy, Canada (Dalrymple et al., 1991). Tidal rhythmites also occur in the late Neoproterozoic glaciogenic succession in South Australia (Williams, 1989a,b,c, 1991), and the deposition of Pennsylvanian estuarine tidal rhythmites in the eastern United States (e.g. Martino and Sanderson, 1993) was coeval with glaciation of Gondwanaland.

Well preserved tidal rhythmites can provide valuable information on palaeotidal periods, the past length of day and the ancient lunar orbit. Tidal rhythmites may record semidiurnal, diurnal and fortnightly periods ascribable to tidal pattern and type, so avoiding some of the uncertainties associated with palaeontological data: for example, diurnal laminae in tidal rhythmites can be related with confidence to the lunar, as opposed to the solar, day. Furthermore, rhythmite facies may span many years, revealing long-term palaeotidal periods not recognisable in fossils.

2.2. Analysis of tidal rhythmite records

An important initial step in the identification of a tidal rhythmite is the correct interpretation of the constituent laminae. A distinctive feature of many tidal rhythmites, as seen in thick neap–spring (fortnightly) cycles from the late Neoproterozoic (~620 Ma) Reynella Siltstone in South Australia, is the presence of *two* graded layers or coarse–fine couplets in many laminae (Fig. 1a). Such laminae and

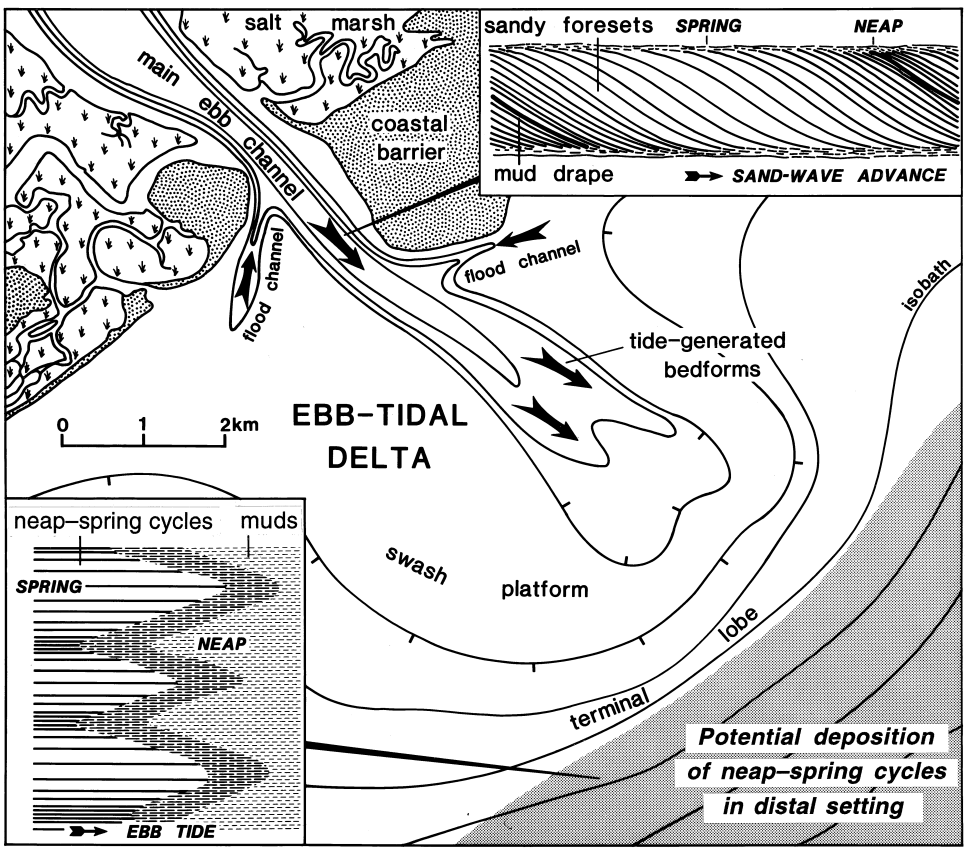

Fig. 2. Envisaged environment of deposition for neap–spring cycles of the Elatina Formation, employing a hypothetical ebb-tidal delta adapted from Imperato et al. (1988). Tidal 'bundle' deposits of cross-bedded sand (top inset) related to bars and sand waves occur in proximal tidal channels, whereas neap–spring cycles of laminated fine sand and silt (shown schematically in bottom inset) are deposited from suspension in a distal setting offshore. Distally, neap–spring cycles become progressively more abbreviated at neaps and eventually pass into shelf muds.

sublaminae usually are interpreted as diurnal and semidiurnal increments, respectively, of the lunar day. The common alternation of thick and thin sublaminae represents the diurnal inequality of a mixed tidal pattern. By contrast, most laminae in rhythmites of the coeval Elatina Formation (Fig. 1b) are interpreted as diurnal increments, although semidiurnal increments occur locally; evidently the tidal ranges and current speeds associated with the weaker semidiurnal constituent usually were too small for much sediment to be transported. Such filtering of high-frequency tidal signals has been observed in other tidal deposits (de Boer et al., 1989). Hence, the identification of tidal rhythmites and their distinction from other types of rhythmite such as varvites may not be straightforward, and a determination of a tidal origin should not rest on the interpretation of a single pattern but rather on a demonstrable self-consistency of a range of patterns and periods.

The geophysical validity of periods and frequencies identified in palaeotidal records of sequential thickness measurements depends greatly on the quality and continuity of the raw data. Long, continuous records provide the best results and are exemplified by the 60-year record of synodic (or lunar) neap–spring cycle thicknesses obtained from drill cores of the Elatina Formation (Williams, 1989a, 1991). This palaeotidal record shows conspicuous cyclicity, with the non-tidal annual oscillation of sea level seen as a periodic variation in the thickness of neap–spring cycles (Fig. 3a,b). Fourier spectral analysis of this record provides a virtually noise-free spectrum

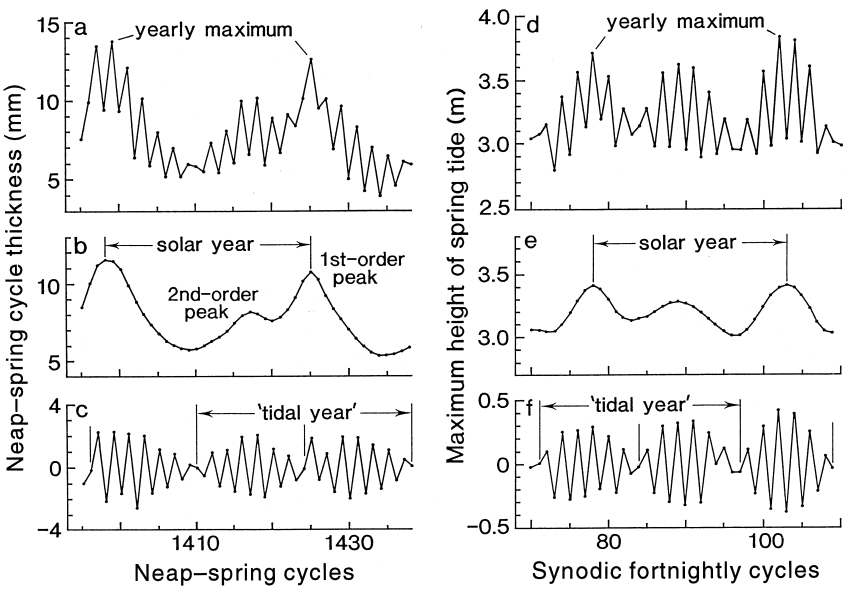

Fig. 3. (a–c) Thickness of fortnightly neap–spring cycles taken from the Elatina tidal rhythmite record, South Australia (neap–spring cycle numbers increase up the stratigraphic succession). (a) Unsmoothed curve, showing annual maxima in thickness. (b) Smoothed curve, showing first-order peaks that define the solar year. (c) Residual curve (a minus b), showing the 'tidal year'; the vertical lines mark 180° phase-reversals in the sawtooth pattern. (d–f) Tidal patterns for Townsville. (d) Maximum height of the fortnightly tidal cycle from 19 October 1968 to 3 June 1970. (e) Smoothed curve, showing the solar year. (f) Residual curve (d minus e), showing the 'tidal year'; the vertical lines mark 180° phase-reversals in the sawtooth pattern.

(Fig. 4b) that may be compared to the spectrum for a 20-year dominantly synodic modern tidal record of spring-tidal heights from Townsville, Queensland (Fig. 4a). The markedly periodic nature of the Elatina record is indicated by the strong, narrow spectral peaks for the annual, semi-annual and monthly periods, and the Townsville spectrum likewise shows clear annual, semi-annual and monthly peaks.

Spectra for incomplete or short records, however, may be misleading, as shown by the spectrum for a 2.8-year record of maximum daily height of sea level at Weipa, Queensland (Fig. 4c). The annual oscillation dominates sea level variation at Weipa but the spectrum has a strong peak at 256 days and peaks representing semi-annual, monthly and fortnightly periods also are shifted to higher frequencies.

Records of diurnal or semidiurnal lamina thicknesses obtained from tidal rhythmites commonly are incomplete because of regular pauses in the deposition of laminae around times of neap tides, when tidal ranges and speeds of tidal currents were low and only mud was deposited for several lunar days. The spectrum for a 4.2-year record of diurnal lamina thicknesses from the Elatina rhythmites (Fig. 4d), whose neap–spring cycles demonstrably are abbreviated at positions of neap tides (Williams, 1989a,b,c, 1991), shows peaks at 333 and 159 diurnal laminae representing the annual oscillation of sea level and the semi-annual tidal cycle, respectively. Further evidence in this spectrum of shifts to higher frequencies is provided by the occurrence of strong peaks at 11.0–12.5 laminae that represent neap–spring cycles, in contrast to direct counts of 14–15 diurnal laminae in apparently unabbreviated neap–spring cycles in rhythmites of the Reynella Siltstone.

Recent claims to have identified palaeotidal periods in lamina-thickness measurements for abbreviated Elatina neap–spring cycles are unjustified. Sonett et al.'s value of 26.2 days/month for the Elatina rhythmites (Sonett et al., 1996a) is invalidated by counts of diurnal laminae in neap–spring cycles of the Reynella rhythmites. Similarly, the spectrum that Archer (1996) obtained for lamina thicknesses of four abbreviated Elatina neap–spring cycles provides no meaningful palaeotidal period because the raw data are corrupted.

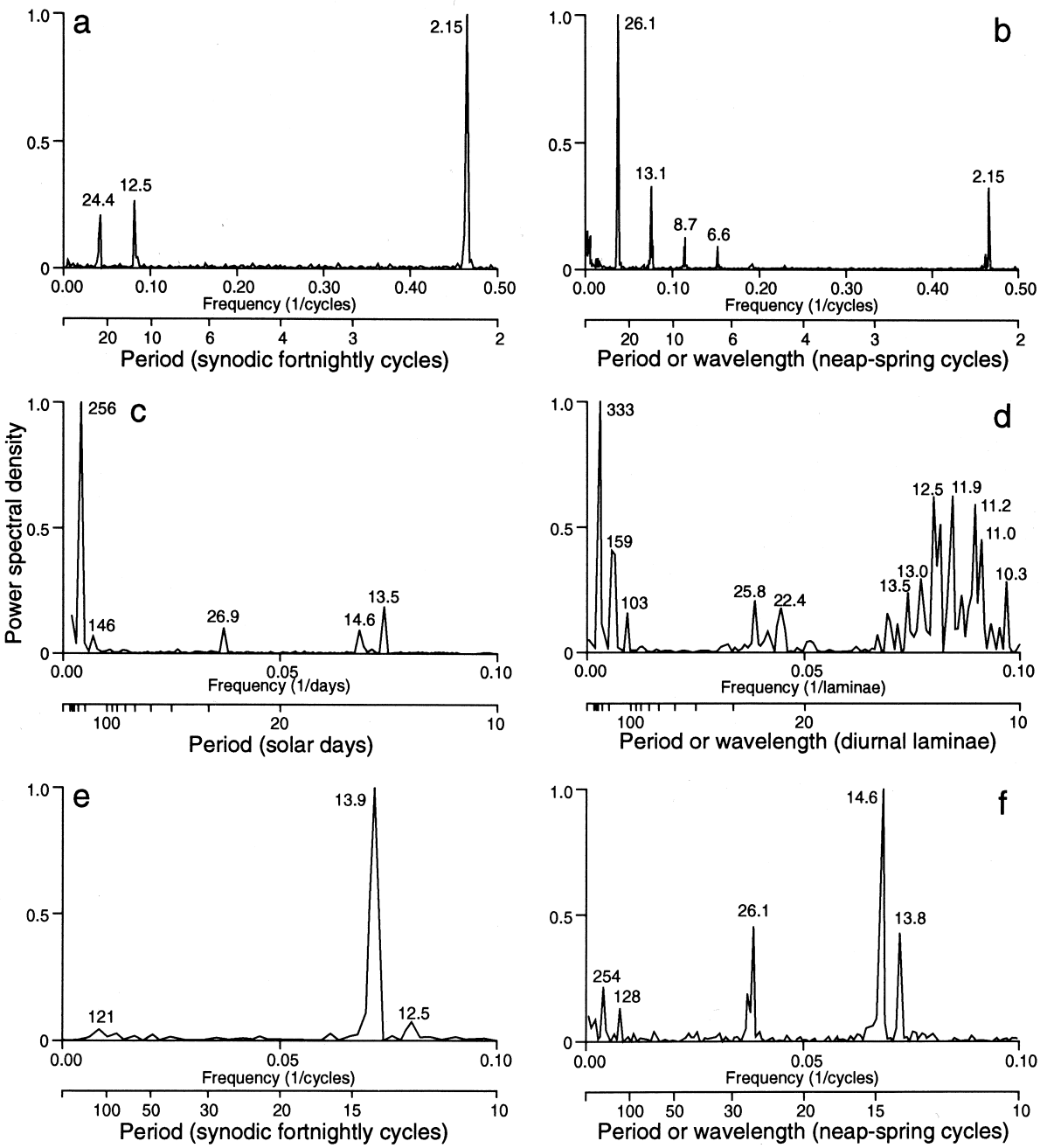

Fig. 4. Fourier transform spectra for tidal and palaeotidal sequential data, with power spectral densities normalised to unity for the strongest peak in each spectrum. (a) Maximum height of 495 synodic spring tides for 20 years from 1 January 1966 to 31 December 1985, for Townsville. The peaks at 24.4 and 12.5 fortnightly cycles represent annual and semi-annual periods, and the peak near 2 fortnightly cycles represents the monthly inequality of spring tides resulting from the ellipticity of the lunar orbit. (b) Continuous, 60-year record of 1580 neap–spring cycle thicknesses from the Elatina rhythmites. The peaks at 26.1 and 13.1 neap–spring cycles represent annual and semi-annual periods, and harmonics at 8.7 and 6.6 cycles the beating among the annual and semi-annual signals and their combination tones. The peak near 2 neap–spring cycles records the monthly inequality of alternate thick and thin neap–spring cycles.

Such abbreviation of the raw data and consequent shifts of spectral peaks must be recognised if tidal-stratigraphic records are to be interpreted correctly. Hence, as discussed in Section 2.4, it is important to conduct tests wherever possible to determine the geophysical validity of claimed palaeotidal and palaeorotational values.

2.3. Neoproterozoic tidal and rotational values

The Elatina–Reynella rhythmites provide a palaeotidal and palaeorotational data set for ~620 Ma (Table 1) that is unequalled for accuracy and completeness. Counts of 14–15 diurnal laminae for apparently unabbreviated neap–spring cycles in the Reynella rhythmites (Fig. 1a) agree with the presence of up to 29 diurnal laminae in successive little-abbreviated neap–spring cycles, representing the synodic month, in the Elatina rhythmites. These numbers suggest 29–30 lunar days/synodic month and in turn imply about 30.5 ± 0.5 solar days/synodic month. Spectral analysis of the 60-year Elatina record shows that the late Neoproterozoic year is represented by 26.1 or 26.2 ± 0.2 neap–spring cycles (the value depending on the method of spectral analysis; Williams, 1989a,b) and contained 13.1 ± 0.1 synodic months. Hence, at ~620 Ma there were 400 ± 7 solar days/year and 21.9 ± 0.4 h/day, assuming negligible change in the length of the year (see Section 2.5).

The period of the lunar nodal cycle (revolution of the Moon's nodes) also is recorded by the Elatina rhythmites. Amplitude-modulation of the semi-annual palaeotidal cycle, as recorded by the second-order peak of the annual cycle (Fig. 3b), indicates a long-term period of 19.5 ± 0.5 years which is interpreted as that of the palaeo-lunar nodal cycle (Williams, 1989a,b,c).

The synodic character of the Elatina palaeotidal pattern is demonstrated in Fig. 5. Dominantly synodic tides such as at Townsville display a characteristic variation in the amplitude of the fortnightly cycle (Fig. 3f and Fig. 5b): (1) alternation of high- and low-amplitude fortnightly cycles to give a 'sawtooth' pattern, or monthly inequality, resulting from the elliptical lunar orbit; (2) systematic modulation of the sawtooth pattern, with 180° changes of phase (i.e. a reversal in the alternation of high- and low-amplitude fortnightly cycles) occurring where the amplitude of the pattern is minimal. As shown in Fig. 5a,b, maximum amplitude of the sawtooth pattern (maximum monthly inequality) occurs when the Earth, Moon and Sun all lie near the major axis of the elliptical lunar orbit; 180° changes of phase of this pattern occur at minimal monthly inequality when all bodies are aligned normal to the major axis. The mean period for a 360° phase-change of the sawtooth pattern, which may be termed the 'tidal year', is 13.95 synodic months (Fig. 4e). This is longer than the solar year of 12.37 synodic months because of the prograde rotation of the lunar perigee (Fig. 5a). Such a synodic pattern is displayed by the Elatina record as a temporal variation in the thickness of neap–spring cycles (Fig. 3c and Fig. 5c); at ~620 Ma the tidal year was 14.6 synodic months (Fig. 4f) and the solar year 13.1 synodic months.

The period of the lunar apsides cycle P_p (the mean duration of a 360° rotation in space of the lunar perigee) is given by:

$$P_p = \frac{Y_t}{Y_t - Y_s} \quad (1)$$

where Y_t and Y_s are the periods of the tidal year and solar year, respectively. At ~620 Ma the lunar apsides period was 9.7 ± 0.1 years.

(c) Maximum daily height of sea level at Weipa for 2.8 years from 5 April 1985. The peaks at 256 and 146 days represent the annual oscillation and the semi-annual tidal cycle, and the peak at 26.9 days the anomalistic month (true period of 27.55 days), at 14.6 days the synodic fortnight (14.77 days) and at 13.5 days the tropical fortnight (13.66 days). (d) Elatina record of 1337 diurnal lamina thickness measurements (4.2-year record, abbreviated at positions of neap tides). Peaks at 333 and 159 diurnal laminae represent the annual oscillation and the semi-annual tidal cycle, and peaks between 10.3 and 13.5 diurnal laminae the neap–spring cycle (cf. 14–15 diurnal laminae per neap–spring cycle obtained from direct counts of the coeval Reynella rhythmites). Peaks at 22.4–25.8 diurnal laminae represent the anomalistic month, also shifted to higher frequencies. (e) Rectified residual record of 493 spring-tidal heights for 1966–1985 for Townsville. The strong period of 13.9 fortnightly cycles modulates the sawtooth pattern in Fig. 3f. (f) Elatina rectified residual record of 1576 neap–spring thickness measurements. The period of 14.6 neap–spring cycles modulates the sawtooth pattern in Fig. 3c; peaks at 26.1 and 13.8 neap–spring cycles represent the annual oscillation and the semi-annual tidal cycle.

Table 1
Palaeotidal and palaeorotational values for Neoproterozoic clastic tidal rhythmites, and modern values

Parameter	~900 Ma [a]	~900 Ma [b]	~620 Ma [c]	Modern
Lunar days/synodic month	(32.0 ± 0.4)	(30.1)	29.5 ± 0.5 [e]	28.53
Solar days/synodic month	(33.0 ± 0.4)	(31.1)	30.5 ± 0.5	29.53
Solar days/sidereal month [f]	(30.9 ± 0.5)	(28.9)	28.3 ± 0.5	27.32
Synodic months/year	(14.6 ± 0.3)	13.47 [e]	13.1 ± 0.1 [e]	12.37
Sidereal months/year [f]	(15.6 ± 0.3)	14.47	14.1 ± 0.1	13.37
Lunar apsides period (years)			9.7 ± 0.1 [e]	8.85
Lunar nodal period (years)			19.5 ± 0.5 [e]	18.61
Solar days/year	481 ± 4	(419.0)	400 ± 7	365.24
Sidereal days/year [f]	482 ± 4	(420.0)	401 ± 7	366.24
Length of solar day (h)	18.2 ± 0.2	(20.9)	21.9 ± 0.4	24.00
Lunar semimajor axis (R_E)	54.1 ± 0.2	(57.18)	58.17 ± 0.30	60.27
Lunar retreat rate (cm/year)	4.38 ± 0.14	(2.19)	2.16 ± 0.31	3.82 ± 0.07 [d]
	900–0 Ma	900–0 Ma	620–0 Ma	laser ranging

Note: The lengths of all tidal and rotational elements vary with time, but the length of the year is taken as constant (see Section 2.5). Values make allowance for the solar tides' contribution to the loss of angular momentum of the Earth's rotation.
[a] Rhythmites of the Big Cottonwood Formation, Utah (Sonett et al., 1996a). Values in brackets derived by the present author from the value of $23.4^{+0.1}_{-0.15}$ *present* solar days/sidereal month given by Sonett et al. (1996a). Errors $\pm 1\sigma$.
[b] Rhythmites of the Big Cottonwood Formation, Utah (corrected primary data; Sonett et al., 1996b). Values in brackets derived by the present author.
[c] Rhythmites of the Elatina Formation–Reynella Siltstone, South Australia (Williams, 1989a,b,c, 1990, 1991, 1994a). Errors $\pm 1\sigma$.
[d] Dickey et al. (1994).
[e] Primary value determined directly from the rhythmite record.
[f] Units in invariable time required for dynamical calculations in Sections 2.5 and 2.6.

Palaeotidal and palaeorotational values, including a length of day of 18.2 ± 0.2 h, derived from rhythmites of the Neoproterozoic (~900 Ma) Big Cottonwood Formation in Utah (Sonett et al., 1996a) also are listed in Table 1 (column 2). Sonett et al.'s (1996a) photograph of the Big Cottonwood rhythmites shows only a few sandstone laminae in each neap–spring cycle and thick muddy neap-tidal bands, implying that the illustrated rhythmite is strongly abbreviated at positions of neap tides. The shortness of the Big Cottonwood neap–spring period of 7.45 laminae (Archer, 1996), which implies a maximum of only ~15 lunar days/month (assuming each lamina represents a lunar day), also argues for an abbreviated record. Subsequently, Sonett et al. (1996b) agreed with the present author that the Big Cottonwood rhythmites they analysed previously are abbreviated at positions of neap tides, and gave a revised value of 13.47 synodic months/year at ~900 Ma based on material they regarded as unabbreviated. That revised value gives a length of day of 20.9 h at ~900 Ma (Table 1, column 3).

2.4. Validity of palaeotidal and palaeorotational values

The geophysical validity of length-of-day estimates can be assessed by testing sets of palaeotidal and palaeorotational values for internal self-consistency by applying the laws of celestial mechanics. This procedure is demonstrated by using *independent* Elatina–Reynella values to determine the lunar semimajor axis (mean Earth–Moon distance) at ~620 Ma.

The lunar nodal period and semimajor axis are related in the expression:

$$P = P_0 \frac{\cos i_0}{\cos i} \left(\frac{a_0}{a}\right)^{1.5} \quad (2)$$

where P_0 is the present lunar nodal period of 18.61 years, P the past lunar nodal period, a_0 the present semimajor axis of 60.27 Earth radii (R_E), a the past lunar semimajor axis, i_0 the inclination of the lunar orbit to the ecliptic of 5.15°, and i the past lunar inclination (Walker and Zahnle, 1986). Assuming negligible evolutionary change in lunar inclination i, a lunar nodal period of 19.5 ± 0.5 years (Table 1)

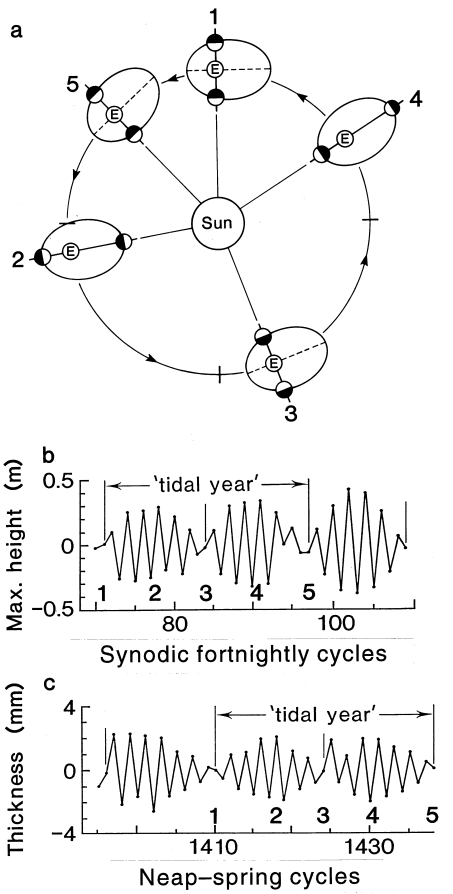

Fig. 5. Synodic fortnightly tidal patterns for one 'tidal year'. (a) Schematic luni–solar conjunctions: 1, 3 and 5, minimum monthly inequality of spring-tidal amplitudes, and phase reversal in the sawtooth pattern of such amplitudes; 2 and 4, maximum monthly inequality. The 'tidal year' (1–5) is longer than the solar year because of prograde rotation of the lunar perigee. (b) Relative amplitude (maximum height) of spring tides at Townsville over one 'tidal year' (see Fig. 3f); nos. 1–5 refer to luni–solar conjunctions shown in (a). (c) Relative thickness of fortnightly neap–spring cycles in the Elatina rhythmite record during one 'tidal year' (see Fig. 3c); nos. 1–5 refer to luni–solar conjunctions shown in (a). The vertical lines in (b) and (c) mark positions of 180° phase-reversals in the sawtooth patterns.

gives $a/a_0 = 0.969 \pm 0.017$ at ~620 Ma (Williams, 1989a).

Kepler's Third Law, which relates a body's orbital period to the dimension of its semimajor axis, can be expressed as:

$$\left(\frac{T}{T_0}\right)^2 = \left(\frac{a}{a_0}\right)^3 \tag{3}$$

where T_0 is the present length of the sidereal month and T is the length of the sidereal month in the past. Taking $T/T_0 = 13.37/(14.1 \pm 0.1)$ from Table 1 gives $a/a_0 = 0.965 \pm 0.005$ at ~620 Ma.

The change in lunar orbital angular momentum and the loss of the Earth's rotational angular momentum through tidal friction of the Moon and the Sun are related in the expression:

$$\left(\frac{a}{a_0}\right)^{1/2} + \frac{(0.46)^2}{13}\left(\frac{a}{a_0}\right)^{13/2} = -\frac{1}{4.93}\frac{\omega}{\omega_0} + 1.219 \tag{4}$$

where ω_0 and ω are the Earth's present and past rotation rates (Deubner, 1990). Taking $\omega_0 = 366.24$ sidereal days and $\omega = 401 \pm 7$ sidereal days (Table 1) gives $a/a_0 = 0.968 \pm 0.007$ at ~620 Ma.

The excellent agreement among the above results for the lunar semimajor axis (Table 2), derived from independent, widely separated rhythmite values and employing three different equations of celestial mechanics that make allowance for lunar and solar tidal effects, demonstrates the self-consistency of the Elatina–Reynella palaeotidal values. Such agreement strongly supports the validity of the implied length of day of 21.9 ± 0.4 h at ~620 Ma.

The estimated length of day of 20.9 h at ~900 Ma (Table 1) cannot be assessed by the above method because the Big Cottonwood data set has only one primary value determined directly from the rhythmite record; other values were derived by employing the primary value in Eqs. 3 and 4. Hence, the estimated length of day at ~900 Ma is unverified.

The mean rate of lunar retreat of 2.16 ± 0.31 cm/year since ~620 Ma indicated by the Elatina–Reynella data set (Table 2) averts a close approach of the Moon at least since 3000 Ma (Williams, 1990, 1994a) and an even lower rate of lunar retreat seems likely during the Proterozoic. The present high rate of lunar retreat of 3.82 ± 0.07 cm/year (Dickey et al., 1994) may imply a near-resonance of the oceans (Lambeck, 1980). Palaeoproterozoic palaeotidal values that are internally self-consistent are required to determine the very early length of day and lunar orbit at a high level of confidence.

Table 2
Lunar semimajor axis (mean Earth–Moon distance) at ~620 Ma and mean rate of lunar retreat for the past ~620 m.y. indicated by tidal rhythmites of the Elatina Formation and Reynella Siltstone (from Williams, 1989a,c, 1990, 1994a; Deubner, 1990)

Palaeotidal/rotational value (Table 1)	Lunar semimajor axis		Mean rate of lunar retreat (cm/year) [a]
	(a/a_0)	(R_E)	
19.5 ± 0.5 years (lunar nodal period)	0.969 ± 0.017	58.40 ± 1.02	1.93 ± 1.06
14.1 ± 0.1 sidereal months/year	0.965 ± 0.005 [c]	58.17 ± 0.30 [c]	2.16 ± 0.31 [c]
401 ± 7 sidereal days/year	0.968 ± 0.007 [b]	58.34 ± 0.42 [b]	1.99 ± 0.43 [b]

[a] Lunar semimajor axis of 385,000 km (Dickey et al., 1994).
[b] Makes allowance for the solar tides' contribution to the loss of angular momentum of the Earth's rotation.
[c] Preferred value based on best-constrained primary data.

2.5. A test of Earth expansion since the Neoproterozoic

The Elatina–Reynella data set (Table 1) can indicate whether the Earth's moment of inertia has changed significantly since ~620 Ma. From Runcorn (1964, 1966):

$$1 - \frac{L}{L_0} = \frac{-1 + \frac{I}{I_0}\frac{\omega}{\omega_0}\frac{Y_0}{Y}}{4.93(1+\beta)} \quad (5)$$

where L/L_0 is the ratio of the past to the present lunar orbital angular momentum (see Runcorn, 1979), I_0 and I are the Earth's present and past moments of inertia, ω_0 and ω are the Earth's present and past rotation rates, Y_0 and Y are the absolute lengths of the present and past sidereal years, β is the present ratio of solar/lunar retarding couples acting on the Earth, and 4.93 represents the present ratio of the Moon's orbital angular momentum to the Earth's spin angular momentum. Assuming that $Y{=}Y_0$ (implying no secular change in the universal gravitational constant G), the Elatina–Reynella palaeotidal and palaeorotational data in Table 1 indicate the following values of I/I_0 for various estimates of β: 1.011 ± 0.018 and 1.018 ± 0.018 ($\beta{=}1/5.5$ and $1/3.7$, respectively; Runcorn, 1966); 1.012 ± 0.018 ($\beta = 1/5.1$; Munk and MacDonald, 1960); 1.014 ± 0.018 ($\beta = 1/4.6$; Lambeck, 1980); and 1.006 ± 0.018 ($\beta = 1/8.2$; Brosche and Wünsch, 1990).

These results represent the only direct estimates of I/I_0 for Precambrian time. They rule out rapid Earth expansion since ~620 Ma by endogenous (non-cosmological) mechanisms, such as Carey's (1976) hypothesis of rapid expansion since the Palaeozoic, which requires $I/I_0 = 0.5$. Nor do the available rhythmite data support slow expansion by endogenous mechanisms; for example, the postulate by Egyed (1969) that the Earth's radius has increased by 0.65 ± 0.15 mm/year for at least the past 600 m.y. gives $I/I_0 = 0.91$–0.94, and an increase in radius proposed by Creer (1965) of 0.50–0.95 mm/year gives $I/I_0 = 0.89$–0.94 (see Runcorn, 1964). The suggestion that significant Earth expansion may have resulted from possible secular decrease in G (Carey, 1976) — that is, $Y \ll Y_0$ — is not supported by studies of the morphologies of Mercury, Mars and the Moon, which show little or no evidence of expansion (Crossley and Stevens, 1976; McElhinny et al., 1978). Furthermore, Mars Viking Lander and lunar laser ranging data indicate negligible change in planetary orbital radii and G (Hellings et al., 1983; Chandler et al., 1993; Dickey et al., 1994). The rhythmite and astrometric observations together militate against significant change in the Earth's radius, either by expansion or contraction, by any mechanism at least since ~620 Ma.

2.6. Resonances of the fluid core for a tidally decelerating Earth

During tidal deceleration of the Earth's rotation, the free nutation or 'tipping' of the fluid core would have undergone resonances with the Earth's semiannual and annual forced nutations caused by luni–solar torques (Toomre, 1974; Hinderer and Legros, 1988; Williams, 1994b). Resonance would occur when:

$$L = 24\left(\frac{Y}{N}\right)^{1/3} \quad (6)$$

where L is the length of day in hours, Y the length of the year in sidereal days, and N the period in sidereal days of the free core nutation as viewed from inertial space. Eq. 6 requires that the absolute length of the year (equivalent to 366.24 present sidereal days) has hardly changed since resonance, a requirement supported by planetary astrometric data (see Section 2.5).

In employing Eq. 6 to estimate possible length of day at resonance, the value of N is taken both as the theoretical (hydrostatic) period of ~460 sidereal days and the presently observed (non-hydrostatic) period of ~430 sidereal days (see Williams, 1994b). These periods give lengths of day of ~22.2 h and ~22.7 h, respectively, for the annual resonance. Taking the length of day of 21.9 h at ~620 Ma given by the Elatina–Reynella rhythmites (Table 1) and assuming a uniform rate of the Earth's despin since that time indicates that the annual resonance would have occurred at $\sim 530 \pm 100$ Ma for the theoretical free core nutation period and at $\sim 380 \pm 70$ Ma for the observed free core nutation period. The stronger, semi-annual resonance would have occurred at an earlier time when the length of day was ~17–18 h. The hypothesis that major tectonothermal reworking events may have resulted from thermal plumes generated at the core–mantle boundary in response to such resonances of the fluid core (Williams, 1994b) may be tested by the acquisition of high-quality palaeorotational data for the Palaeoproterozoic.

3. Glaciogenic deposits

3.1. Discrimination of glaciogenic and impact ejecta deposits

Early debates concerning a glacial versus a density flow or slump origin of diamictites (Crowell, 1957; Schermerhorn, 1974) have long been resolved, with a glacial interpretation remaining intact for the majority of deposits under scrutiny. Sedimentologists recognise that the presence of diamictite alone does not indicate a glacial origin. However, many glaciogenic sediments have been reworked by gravity-flow processes including submarine debris flows (see Eyles, 1993), and some Precambrian diamictites formerly regarded as tillites have been reinterpreted as non-glaciogenic debris-flow deposits of subaqueous (Jensen and Wulff-Pedersen, 1996) and continental (Williams and Schmidt, 1996) origin.

Recently it has been argued that some diamictites widely regarded as tillites should be reassessed as possible ejecta from impacts with Earth-crossing asteroids and comets (e.g. Oberbeck et al., 1993), although such claims are sweeping and unsupported by observation (see Young, 1993; le Roux, 1994). Important features of glacial–periglacial successions of Precambrian age and impact ejecta deposits are listed in Table 3. Late Neoproterozoic strata in the Adelaide foldbelt region in South Australia (Fig. 6) permit the comparison of glacial–periglacial deposits and a stratigraphically and sedimentologically distinct impact ejecta horizon (Fig. 7; Gostin et al., 1986; Wallace et al., 1996) that can be linked to Acraman, Australia's largest known complex impact structure located ~300–400 km west of the Adelaide foldbelt (Williams, 1986b, 1994d; Schmidt and

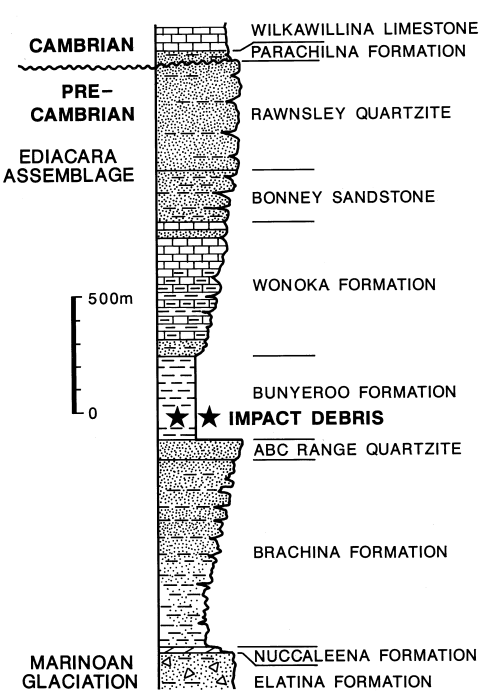

Fig. 6. Stratigraphic section of late Neoproterozoic strata exposed along the western margin of the central Adelaide foldbelt (Geosyncline), showing the position of the impact ejecta horizon within shales of the Bunyeroo Formation ~1000 m stratigraphically above the glaciogenic Elatina Formation which includes tidal rhythmites. After Gostin et al. (1986).

Table 3
Features of Precambrian glacial–periglacial successions and impact ejecta deposits

Glacial–periglacial successions
Striated and polished bedrock pavements [a] commonly showing multiple directions of striations and grooves, chattermarks, roche moutonnées and associated erosional forms
Faceted, polished and striated clasts with multiple directions of striations [a], in polymictic diamictites [a]
Chemically precipitated iron-formations [a], laminated mudstones [a] and tidal rhythmites [a] containing faceted and striated dropstones [a] over stratigraphic intervals representing months to many years [a]
Till pellets [a] (Ovenshine, 1970)
Periglacial structures in related permafrost regolith [a], including sand-wedge polygons [a] (patterned ground)
Cyclic repetition of diamictite and associated facies [a]
Very thick successions (up to 4000 m) [a]
Successions correlative over continent-wide distances (up to 3000 km)[a]
Deposits commonly reworked by subaqueous gravity-flow mechanisms [a]
Impact ejecta deposits
Striated and polished bedrock below proximal breccia near an identifiable impact structure
Abundant angular clasts [b]
Shatter cones in angular clasts [b]
Planar shock lamellae in multiple sets common in quartz [b] and feldspar grains [b]
Other mineral grains strongly fractured [b]
High-pressure phases of silica (usually preserved only for relatively young impacts)
Abundant glassy spherules or devitrified melt particles [b]
Iridium [b] and other platinum group element [b] geochemical anomalies
Thick (up to 2000 m) proximal coarse breccia deposits not widely distributed, and are in close proximity to an identifiable impact structure
Non-linear decrease in thickness with radial distance from the source crater [b]
Thin distal deposits widespread and laterally continuous as a single horizon [b]
Deposits commonly reworked by tsunamis [b]

[a] Identified in Neoproterozoic (~725–620 Ma) glaciogenic successions in the Adelaide foldbelt (Link and Gostin, 1981; Williams, 1986a, 1994c; Preiss, 1987; Young and Gostin, 1991).
[b] Identified in the late Neoproterozoic (~590 Ma) Acraman impact ejecta horizon in the Adelaide foldbelt (Gostin et al., 1986, 1989; Wallace et al., 1990, 1996).

Williams, 1996). In addition to clear differences between the glaciogenic and impact-generated facies (Table 3), the thicknesses of up to 4000 m attained by the glaciogenic successions over wide areas cannot plausibly be explained by the ejecta hypothesis. Impact ejecta deposits show a non-linear decrease in thickness with radial distance from the source crater centre; over a wide range of scales, ejecta blanket thickness t decreases with distance r from the crater centre as:

$$t = 0.14R^{0.74}\left(\frac{r}{R}\right)^{-3.0} \quad \text{for } r \geq R \tag{7}$$

where R is the transient crater (not final collapse crater) radius and all dimensions are in metres (McGetchin et al., 1973; Melosh, 1989). Employing Eq. 7, a transient crater radius of 2.0×10^4 m (40 km diameter; Williams, 1994d) for Acraman gives thicknesses for undisturbed ejecta of 7.8 cm at a distance of 280 km from the crater centre, 5.8 cm (309 km), 3.7 cm (358 km) and 3.0 cm (385 km). These predicted thicknesses are of the same order as observed thicknesses for the distal ejecta horizon in the Adelaide foldbelt (Fig. 7). With regard to proximal ejecta for a crater the size of Acraman, a fully preserved and undisturbed breccia deposit 1000 m thick would be only 11 km from the crater centre, and hence would be fallback breccia within the excavated area; a breccia deposit 500 m thick would be fallback only 15 km from the crater centre; and a breccia deposit 100 m thick would be 25.7 km from the crater centre and so just outside the excavated area. To produce, by impact, the great thicknesses and 3000-km extent of correlative diamictites across Australia would require numerous penecontemporaneous impacts of the same magnitude as Acraman within and bordering Neoprotero-

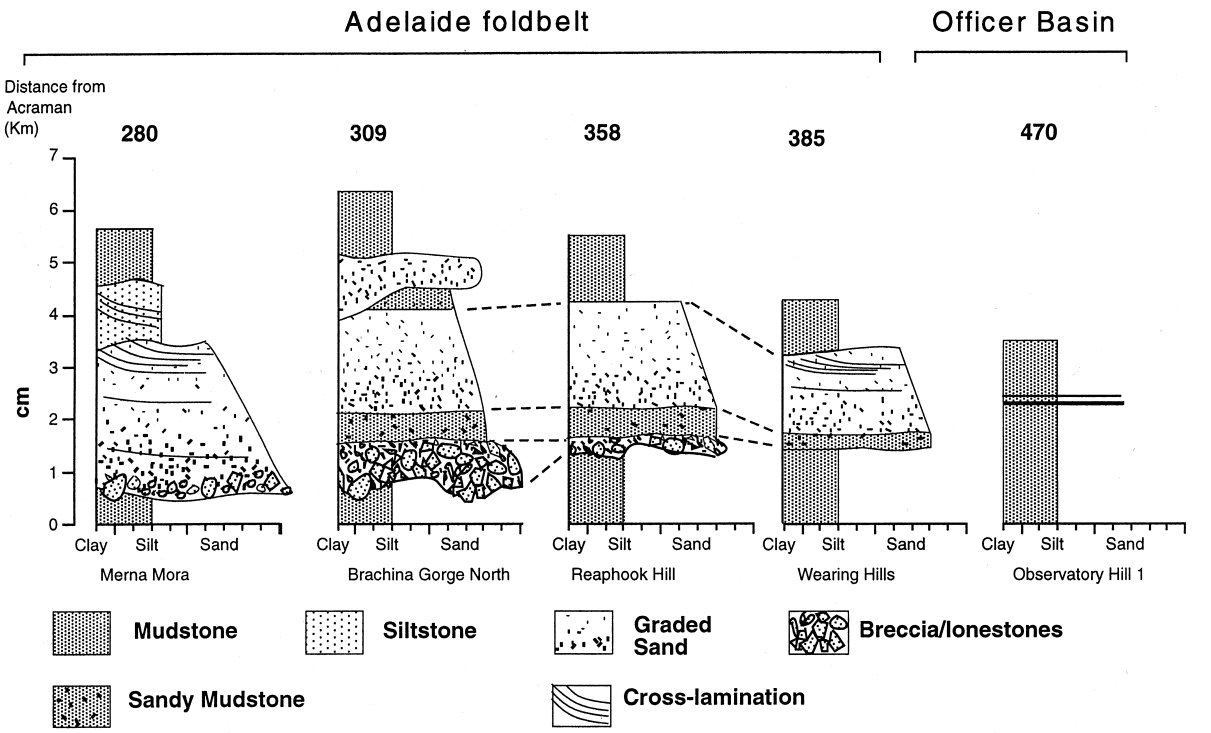

Fig. 7. Representative sections of the impact ejecta horizon in the Adelaide foldbelt and Officer Basin, South Australia, arranged according to radial distance from the Acraman impact structure. Modified from Wallace et al. (1996).

zoic basins across Australia. No evidence exists for such impacts.

Although identified proximal impact ejecta breccias locally attain thicknesses of 2000 m (Poag and Aubry, 1995; Witzke and Anderson, 1996), the breccia facies is distinctive. The distal ejecta horizon in the Adelaide foldbelt (Fig. 7) typically comprises a breccia–sandy mudstone–graded sandstone succession reflecting different transport modes: fireball processes or ejecta flows for the breccia and atmospheric processes such as air-blast for the sand (Wallace et al., 1996). Nearer the impact site these facies are reworked by impact-induced tsunami activity. Evidence of tsunamis, such as reworking, rip-up clasts and cross-bedding, is seen in ejecta deposits associated with other impact structures (e.g. Alvarez et al., 1992; Steiner and Shoemaker, 1996).

In conclusion, careful observation in the field and laboratory should permit glaciogenic and impact ejecta deposits to be readily distinguished. However, impact with Earth-crossing bodies is an important geological process and geologists should be familiar with criteria indicative of impact because it is virtually certain that the stratigraphic record contains undiscovered ejecta deposits.

3.2. Palaeomagnetism of glaciogenic successions and the Precambrian climatic paradox

Recent research on the palaeomagnetism of Precambrian glaciogenic successions in Australia and other continents is challenging one of the tenets of palaeoclimatology — that past glaciation near sea level was circumpolar.

Palaeomagnetism is a powerful tool in palaeoenvironmental studies and the procedures (Butler, 1992) should be understood by sedimentologists. Depositional and post-depositional detrital remanent magnetisation (DRM) acquired during or soon after deposition by the orientation of detrital magnetic particles such as magnetite and specular hematite in the ambient geomagnetic field can give a reliable indication of palaeolatitude, provided that samples are taken over a stratigraphic interval sufficient to

permit secular variation of the magnetic field to be averaged out. Hematitic red beds commonly acquire a stable, chemical remanent magnetisation (CRM) during early diagenesis (Turner, 1980). Field tests such as fold (tectonic, soft-sediment) and conglomerate tests are applied where possible to constrain the timing of magnetic remanence and so distinguish primary from overprint components of magnetisation. Components are revealed by stepwise demagnetisation (thermal, alternating field, chemical), followed by principal component analysis (Kent et al., 1983) whereby linear segments are fitted to data points in plots of orthogonal projections, the data points being weighted according to the inverse of their measured variances. Palaeomagnetic studies employ the geocentric axial dipole hypothesis for the geomagnetic field, which holds that the time-averaged position of the geomagnetic pole is close to the Earth's rotation axis (Butler, 1992). Former geographic latitude or palaeolatitude λ is obtained by applying the dipole formula $\tan I = 2\tan\lambda$, where I is the mean palaeomagnetic inclination. Hence the palaeolatitude is always less than I (except for $I = 90^{o}$), and for $I \leq 40^{o}$ the palaeolatitude is only about half the value of I.

The palaeolatitude of Precambrian glaciations has been contentious since Harland and Bidgood (1959) suggested that Neoproterozoic glaciation in Norway occurred in low palaeolatitudes. Other early palaeomagnetic studies of Neoproterozoic glaciogenic rocks in Greenland, Scotland, Canada, Australia and South Africa also suggested low palaeolatitudes of glaciation, although some of the data were equivocal or contentious. Meert and Van der Voo (1994) attempted to resolve the enigma by claiming that *all* the palaeomagnetic data are overprints, and concluded that Neoproterozoic glaciation did not extend equatorward of 25° palaeolatitude. Some of the early data undoubtedly are spurious. However, recent palaeomagnetic studies indicate that deposits of the Marinoan (~620 Ma) glaciation in South Australia, which appears to be broadly coeval with the Varanger glaciation in the North Atlantic region (see Hambrey and Harland, 1981), formed near the palaeoequator ($\lambda = 2.7^{o} \pm 3.7^{o}$; Schmidt et al., 1991; Schmidt and Williams, 1995). This finding is supported by positive palaeomagnetic fold tests on small folds that demonstrably are of soft-sediment origin (Williams, 1996), thus confirming DRM, and by high-quality palaeomagnetic data for contiguous strata in the Adelaide foldbelt (Schmidt and Williams, 1996). Furthermore, Park (1997) showed that Rapitan glaciomarine episodes (~725 Ma) in northwestern Canada, which are broadly correlative with the Sturtian glaciation in South Australia, took place at palaeolatitudes of $6^{o} \pm 4^{o}$ and $4^{o} \pm 6^{o}$.

Palaeomagnetic data for Palaeoproterozoic glaciogenic strata also suggest low palaeolatitudes of deposition. The glaciomarine Coleman Member of the ~2300-Ma Gowganda Formation (Huronian) in Ontario, Canada (Young, 1981; Miall, 1983), evidently accumulated near the palaeoequator (Williams and Schmidt, 1997). Evans et al. (1997) obtained a palaeolatitude of $11^{o} \pm 5^{o}$ for ~2200-Ma volcanics overlying the glaciogenic Makganyene diamictite in South Africa and inferred a low palaeolatitude of glaciation. In addition, palaeomagnetic data suggest that the Hamersley Basin in northwestern Australia was near the palaeoequator at ~2200 Ma when the glaciogenic Meteor Bore Member of the Turkey Creek Formation was deposited (see Schmidt and Clark, 1994). Palaeomagnetically determined low latitudes evidently do not reflect non-dipole behaviour of the geomagnetic field because the morphology of the geomagnetic field has been tested (Evans, 1976; Piper and Grant, 1989) and found to be more consistent with a dipole configuration than with other multi-pole configurations back to 3000 Ma.

Sedimentological studies of Marinoan glaciogenic rocks have provided evidence of grounded glaciers and glaciomarine deposition (Lemon and Gostin, 1990), the latter confirmed by the presence of tidal rhythmites (Williams, 1989a,b,c, 1991). Dolostones closely associated with Marinoan and Varanger glaciogenic deposits (e.g. Williams, 1979; Fairchild and Hambrey, 1984; Kennedy, 1996) may record rapid and profound changes of climate. Periglacial contraction–expansion sand-wedge polygons in a Marinoan permafrost horizon indicate in situ cold climate near sea level and marked seasonality (mean monthly air temperatures ranging from -35°C or lower in midwinter to $< +4$°C in midsummer; Williams, 1986a, 1994c). Cross-stratal attitudes in associated periglacial aeolianite imply the movement of cold, dry palaeowinds obliquely toward or across

the palaeoequator (Williams, 1998). A frigid Neoproterozoic climate near sea level in low palaeolatitudes is all the more paradoxical because the faster rotation of the Earth (21.9-h day at ~620 Ma and 20.9-h day at ~900 Ma; Table 1) would have caused less efficient poleward transport of heat, resulting in cooler poles and warmer equatorial regions (Kuhn et al., 1989; Jenkins, 1996).

Palaeomagnetic and sedimentological research is thus revealing *the Precambrian climatic paradox* of frigid strongly seasonal climate, grounded glaciers and permafrost near sea level in low to equatorial palaeolatitudes. The latitudinal distribution of episodic cold climate in the Precambrian evidently differed markedly from that of the Phanerozoic.

3.3. Possible causes of low-palaeolatitude glaciation

The jury is still out on possible explanations of the paradoxical Precambrian glacial climate (see Williams, 1994c). However, the claim that past major glaciations, including Neoproterozoic glaciations in low palaeolatitudes, were initiated by uplift related to rifting and orogeny (Eyles, 1993) is difficult to support. Most estimates of maximum crustal uplift associated with hotspot swells and rifting are in the range of 0.5–1.5 km (e.g. Crough, 1983; Hill et al., 1992), and as the modern snowline elevation is 4 to 5.5 km for latitudes $<30^{\circ}$ (Eyles, 1993), rifting is not a viable explanation for Neoproterozoic glaciomarine deposition and cold climate near sea level in low palaeolatitudes. Furthermore, Marinoan glaciation in South Australia, which saw permafrost develop near sea level on the cratonic Stuart Shelf, was unrelated to mountain building.

Foremost among other explanations for low-palaeolatitude glaciation near sea level are global (pole-to-pole) glaciation or 'snowball Earth' caused by global refrigeration (Harland, 1964; Kirschvink, 1992), and the 'large obliquity' hypothesis of preferential low-latitude glaciation under a strongly seasonal climate (Williams, 1975, 1993). However, these hypotheses also face obstacles.

Although global refrigeration may seem a ready explanation for low-palaeolatitude glaciation, computer modelling indicates that it would not produce ice sheets near the equator. Crowley and Baum (1993) found that the ice margin limit would have been at 25° latitude, taking a late Neoproterozoic solar luminosity at 6% less than at present and employing the most favourable continental configuration. Walsh and Sellers (1993) found that with a 30% decrease in the solar constant the oceans would freeze over but that the limit of permanent snow and ice on land would be well short of the equator "because the oceans were no longer able to supply the water vapour needed to sustain the snowfall rates needed for the further advance of the snow cover over land". Importantly, there would be little seasonal variation for such a frozen Earth because the very low temperatures would inhibit precipitation and sublimation (Sellers, 1990). Moreover, a frozen-over Earth would be very difficult to unfreeze, which may require a dramatic increase in solar luminosity (see North et al., 1981) or some other catastrophic event. From a geological viewpoint, the Neoproterozoic stratigraphic record (e.g. Preiss, 1987) shows no evidence of the drastic lowering of sea level that would be expected if global ice sheets existed at that time.

Alternatively, a large obliquity of the ecliptic offers a possible explanation for the paradoxical character of Precambrian glaciations. The Earth's obliquity or axial tilt (now 23.5°) controls the sign and strength of climatic zonation, and an obliquity $>54^{\circ}$ would cause low latitudes ($\leq 30^{\circ}$) to receive less solar radiation annually than either pole (Fig. 8). The intensity of seasonality also increases with increase in obliquity. If an Earth with an obliquity $>54^{\circ}$ were to enter an ice age through some independent cause such as a decrease in atmospheric p_{CO_2} — a large obliquity by itself is not a cause of glaciation — low latitudes ($\leq 30^{\circ}$) would be glaciated preferentially; also, the global seasonal cycle would be intense and zonal surface winds would be reversed. Such features are suggested by some Precambrian glaciogenic successions. This hypothesis, however, also must explain: (1) how the Earth acquired a large Precambrian obliquity; and (2) a necessary reduction of obliquity during the latest Neoproterozoic–early Palaeozoic to accommodate the *high*-palaeolatitude glaciations of the Palaeozoic. These two requirements are investigated below.

The study of Hartmann and Vail (1986) implies that a giant impact of the proto-Earth with a planet-sized body (impactor of 0.15 Earth-masses; Taylor

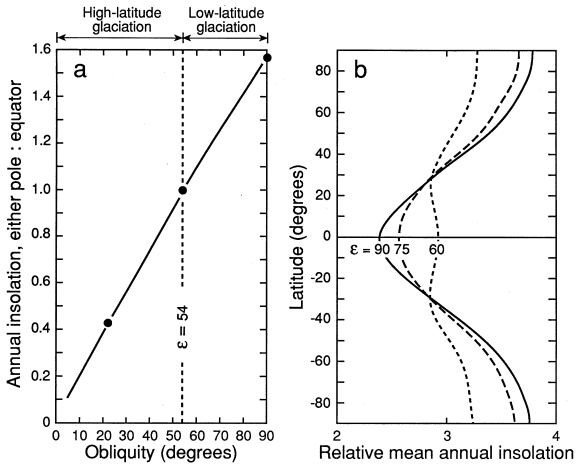

Fig. 8. (a) Relation between the obliquity of the ecliptic ε and the ratio of annual insolation at either pole to that at the equator (solid line); the dashed line at $\varepsilon = 54^{o}$ separates the fields of preferential low-latitude and high-latitude glaciation. (b) Latitudinal variation of relative mean annual insolation of a planet for various values of obliquity (ε, in degrees). The plots in (a) and (b) together show that for $\varepsilon > 54^{o}$, glaciation would occur preferentially in low latitudes. From Williams (1993).

and Esat, 1996), which most astronomers now believe explains the origin and angular momentum of the Earth–Moon system, most probably would result in a large obliquity ($>60^{o}$) for the early Earth. Furthermore, Dones and Tremaine (1993) noted that the obliquity of a planet resulting from impacts by a few large bodies "is likely to be substantial" and gave probabilities of 0.73 to 0.91 that a single giant impact would have induced an obliquity $>24^{o}$ for the early Earth. These new dynamical concepts conflict with the earlier view (e.g. Goldreich, 1966) that the early Earth's obliquity was small ($<23^{o}$), and permit a large mean obliquity during the Precambrian.

Possible mechanisms for secular reduction of obliquity since the late Neoproterozoic remain to be explored. For example, reduction in obliquity caused by core–mantle dissipation (Williams, 1993), which would have increased greatly during the annual resonance of the fluid core (see Section 2.6), is unquantified. Change in the mass distribution of the Earth caused by mass transport between oceans and high-latitude ice sheets, together with planetary perturbations and luni–solar torques acting on the Earth's oblate figure, also may cause secular change of obliquity. Bills (1994) argued that feedback in such a system may cause the obliquity to change at a rate of up to $55^{o}/100$ m.y., although the proposed high rate of change has been challenged (Peltier and Jiang, 1994). Rubincam (1995) termed this mechanism 'climate friction' and suggested that secular increase in obliquity by such means may explain the Earth's present tilt. Ito et al. (1995) estimated a rate of increase in obliquity of $0.4^{o}/10$ m.y. through climate friction, the rate and sign of change depending on values taken for the viscosity of the lower mantle, the extent of polar ice-sheet development, and lag times for the growth and decay of ice sheets and for solid Earth deformation. All these studies assume that the Earth's former obliquity was smaller than the present value and that past ice sheets were circumpolar and can be represented in models as excess mass symmetrically placed at the poles. However, such assumptions may not be valid for the Precambrian Earth, and no investigation has been made of the dynamical effects of the growth and decay of low-latitude ice sheets, particularly for the case where such ice sheets are asymmetrically disposed with respect to the spin axis.

The explanations of low-palaeolatitude glaciation may be tested by interdisciplinary research. Global glaciation implies that episodic glaciation during the Precambrian invariably would have affected high palaeolatitudes and also low palaeolatitudes at times of extreme glacial advance. On the other hand, the large-obliquity hypothesis implies that all Precambrian glaciations *near sea level* back to $\geq$2500 Ma should be confined to low palaeolatitudes ($\leq 30^{o}$). Hence, these two hypotheses may be tested by determining the palaeolatitude and palaeoenvironment of Precambrian glaciogenic deposits and seeking indications of seasonality and other palaeoclimatic features. The determination of Precambrian palaeowind directions relative to palaeolatitudes may provide another test, although the palaeomagnetic data must be linked to a reliable apparent polar wander path that extends to the Cenozoic and unambiguously defines geographic polarity. Accurate age determinations of Neoproterozoic glaciogenic rocks also may illuminate the cause of low-palaeolatitude glaciation: global refrigeration predicts synchronous glacial successions in low palaeolatitudes, whereas broad diachronism of glaciogenic successions would be possible with movement of continents across low

latitudes for a large obliquity, although synchronism of successions is not precluded.

4. Conclusions

Through studies of tidal and glacial deposits, clastic sedimentology can contribute substantially to understanding Precambrian Earth–Moon dynamics and global environments.

The study of Precambrian clastic tidal rhythmites has provided palaeotidal and palaeorotational data. Palaeotidal records commonly are abbreviated at positions of neap tides, however, and such data should be viewed as unverified until successfully tested for self-consistency through application of the laws of celestial mechanics. Verified values for the late Neoproterozoic Elatina–Reynella rhythmites indicate a length of day of 21.9 h at ~620 Ma and a mean rate of lunar retreat of 2.16 cm/year since that time. The Elatina–Reynella data set does not support significant change in the Earth's radius at least since the late Neoproterozoic, and suggests that the Earth's fluid core may have undergone a major resonance during the latest Neoproterozoic–early Palaeozoic.

Palaeomagnetic data based on the geocentric axial dipole model for the geomagnetic field show that the climatic paradox of glaciation and cold climate near sea level in low palaeolatitudes, first established for the late Neoproterozoic, applies also to the Palaeoproterozoic. Possible explanations of this enigma, including global glaciation and an increased obliquity of the ecliptic, require continuing multidisciplinary research. The palaeogeographic distribution of Precambrian ice sheets is relevant to modelling the influence of obliquity–oblateness feedback mechanisms on the Earth's obliquity history.

Acknowledgements

I thank Phil Schmidt for collaborative research on Precambrian palaeomagnetism, Vic Gostin for comments on an early draft of the manuscript and for providing Fig. 6, Malcolm Wallace for providing Fig. 7, and Mike Hambrey and Carel Snyman for constructive reviews. Tidal data for Weipa and Townsville were provided by the Beach Protection Authority, Queensland Department of Transport, through the National Tidal Facility, Adelaide. The work is supported by an Australian Research Council Senior Research Fellowship.

References

Alvarez, W., Smit, J., Lowrie, W., Asaro, F., Margolis, S.V., Claeys, P., Kastner, M., Hildebrand, A.R., 1992. Proximal impact deposits at the Cretaceous–Tertiary boundary in the Gulf of Mexico: A restudy of DSDP Leg 77 Sites 536 and 540. Geology 20, 697–700.

Archer, A.W., 1996. Reliability of lunar orbital periods extracted from ancient cyclic tidal rhythmites. Earth Planet. Sci. Lett. 141, 1–10.

Bills, B.G., 1994. Obliquity–oblateness feedback: Are climatically sensitive values of obliquity dynamically unstable? Geophys. Res. Lett. 21, 177–180.

Brosche, P., Wünsch, J., 1990. The solar torque — a leak for the angular momentum of the Earth–Moon system. In: Brosche, P., Sündermann, J. (Eds.), Earth's Rotation from Eons to Days. Springer, Berlin, pp. 141–145.

Butler, R.F., 1992. Paleomagnetism: Magnetic Domains to Geologic Terranes. Blackwell, Oxford, 319 pp.

Carey, S.W., 1976. The Expanding Earth. Elsevier, Amsterdam, 488 pp.

Chan, M.A., Kvale, E.P., Archer, A.W., Sonett, C.P., 1994. Oldest direct evidence of lunar–solar tidal forcing in sedimentary rhythmites. Proterozoic Big Cottonwood Formation, central Utah. Geology 22, 791–794.

Chandler, J.F., Reasenberg, R.D., Shapiro, I.I., 1993. New bound on G. Bull. Am. Astron. Soc. 25, 1233.

Creer, K.M., 1965. An expanding Earth? Nature 205, 539–544.

Crossley, D.J., Stevens, R.K., 1976. Expansion of the Earth due to a secular decrease in G —evidence from Mercury. Can. J. Earth Sci. 13, 1723–1725.

Crough, S.T., 1983. Hotspot swells. Annu. Rev. Earth Planet. Sci. 11, 165–193.

Crowell, J.C., 1957. Origin of pebbly mudstones. Geol. Soc. Am. Bull. 68, 993–1009.

Crowley, T.J., Baum, S.K., 1993. Effect of decreased solar luminosity on late Precambrian ice extent. J. Geophys. Res. 98, 16723–16732.

Dalrymple, R.W., Makino, Y., Zaitlin, B.A., 1991. Temporal and spatial patterns of rhythmite deposition on mud flats in the macrotidal Cobequid Bay–Salmon River estuary, Bay of Fundy, Canada. Can. Soc. Pet. Geol. Mem. 16, 137–160.

De Boer, P.L., Oost, A.P., Visser, M.J., 1989. The diurnal inequality of the tide as a parameter for recognizing tidal influences. J. Sediment. Petrol. 59, 912–921.

Deubner, F.-L., 1990. Discussion on Late Precambrian tidal rhythmites in South Australia and the history of the Earth's rotation. J. Geol. Soc. London 147, 1083–1084.

Deynoux, M., Duringer, P., Khatib, R., Villeneuve, M., 1993. Laterally and vertically accreted tidal deposits in the Upper Proterozoic Madina-Kouta Basin, southeastern Senegal, West Africa. Sediment. Geol. 84, 179–188.

Deynoux, M., Miller, J.M.G., Domack, E.W., Eyles, N.,

Fairchild, I.J., Young, G.M. (Eds.), 1994. Earth's Glacial Record. Cambridge University Press, Cambridge, 266 pp.

Dickey, J.O., Bender, P.L., Faller, J.E., Newhall, X.X., Ricklefs, R.L., Ries, J.G., Shelus, P.J., Veillet, C., Whipple, A.L., Wiant, J.R., Williams, J.G., Yoder, C.F., 1994. Lunar laser ranging: a continuing legacy of the Apollo program. Science 265, 482–490.

Dones, L., Tremaine, S., 1993. Why does the Earth spin forward? Science 259, 350–354.

Egyed, L., 1969. The slow expansion hypothesis. In: Runcorn, S.K. (Ed.), The Application of Modern Physics to the Earth and Planetary Interiors. Wiley Interscience, London, pp. 65–75.

Evans, D.A., Beukes, N.J., Kirschvink, J.L., 1997. Low-latitude glaciation in the Palaeoproterozoic era. Nature 386, 262–266.

Evans, M.E., 1976. Test of the dipolar nature of the geomagnetic field throughout Phanerozoic time. Nature 262, 676–677.

Eyles, N., 1993. Earth's glacial record and its tectonic setting. Earth-Sci. Rev. 35, 1–248.

Fairchild, I.J., Hambrey, M.J., 1984. The Vendian succession of northeastern Spitsbergen: petrogenesis of a dolomite–tillite association. Precambrian Res. 26, 111–167.

Goldreich, P., 1966. History of the lunar orbit. Rev. Geophys. 4, 411–439.

Gostin, V.A., Haines, P.W., Jenkins, R.J.F., Compston, W., Williams, I.S., 1986. Impact ejecta horizon within late Precambrian shales, Adelaide Geosyncline, South Australia. Science 233, 198–200.

Gostin, V.A., Keays, R.R., Wallace, M.W., 1989. Iridium anomaly from the Acraman impact ejecta horizon: impacts can produce sedimentary iridium peaks. Nature 340, 542–544.

Hambrey, M.J., Harland, W.B. (Eds.), 1981. Earth's pre-Pleistocene Glacial Record. Cambridge University Press, Cambridge, 1004 pp.

Harland, W.B., 1964. Critical evidence for a great Infra-Cambrian glaciation. Geol. Rundsch. 54, 45–61.

Harland, W.B., Bidgood, D.E.T., 1959. Palaeomagnetism in some Norwegian sparagmites and the late Pre-Cambrian ice age. Nature 184, 1860–1862.

Hartmann, W.K., Vail, S.M., 1986. Giant impactors: plausible sizes and populations. In: Hartmann, W.K., Phillips, R.J., Taylor, G.J. (Eds.), Origin of the Moon. Lunar and Planetary Institute, Houston, TX, pp. 551–566.

Hellings, R.W., Adams, P.J., Anderson, J.D., Keesey, M.S., Lau, E.L., Standish, E.M., Canuto, V.M., Goldman, I., 1983. Experimental test of the variability of *G* using Viking Lander ranging data. Phys. Rev. Lett. 51, 1609–1612.

Hill, R.I., Campbell, I.H., Davies, G.F., Griffiths, R.W., 1992. Mantle plumes and continental tectonics. Science 256, 186–193.

Hinderer, J., Legros, H., 1988. Tidal flow in the Earth's core: a search for the epoch and amplitude of exact resonance in the past. Geophys. Monogr. 46, 79–82.

Imperato, D.P., Sexton, W.J., Hayes, M.O., 1988. Stratigraphy and sediment characteristics of a mesotidal ebb-tidal delta, North Edisto Inlet, South Carolina. J. Sediment. Petrol. 58, 950–958.

Ito, T., Masuda, K., Hamano, Y., Matsui, T., 1995. Climate friction: A possible cause for secular drift of Earth's obliquity. J. Geophys. Res. 100, 15147–15161.

Jenkins, G.S., 1996. A sensitivity study of changes in Earth's rotation rate with an atmospheric general circulation model. Global Planet. Change 11, 141–154.

Jensen, P.A., Wulff-Pedersen, E., 1996. Glacial or non-glacial origin for the Bigganjargga tillite, Finnmark, northern Norway. Geol. Mag. 133, 137–145.

Kennedy, M.J., 1996. Stratigraphy, sedimentology, and isotopic geochemistry of Australian Neoproterozoic postglacial cap dolostones: deglaciation, $\delta^{13}C$ excursions, and carbonate precipitation. J. Sediment. Res. 66, 1050–1064.

Kent, J.T., Briden, J.C., Mardia, K.V., 1983. Linear and planar structure in ordered multivariate data as applied to progressive demagnetization of palaeomagnetic remanence. Geophys. J. R. Astron. Soc. 75, 593–621.

Kirschvink, J.L., 1992. Late Proterozoic low-latitude global glaciation: The snowball Earth. In: Schopf, J.W., Klein, C. (Eds.), The Proterozoic Biosphere: A Multidisciplinary Study. Cambridge University Press, Cambridge, pp. 51–52.

Kuhn, W.R., Walker, J.C.G., Marshall, H.G., 1989. The effect on Earth's surface temperature from variations in rotation rate, continent formation, solar luminosity, and carbon dioxide. J. Geophys. Res. 94, 11129–11136.

Lambeck, K., 1980. The Earth's Variable Rotation: Geophysical Causes and Consequences. Cambridge Univ. Press, Cambridge, 449 pp.

Lemon, N.M., Gostin, V.A., 1990. Glacigenic sediments of the late Proterozoic Elatina Formation and equivalents, Adelaide Geosyncline, South Australia. Geol. Soc. Aust. Spec. Publ. 16, 149–163.

Le Roux, J.P., 1994. Impacts, tillites, and the breakup of Gondwanaland: a second discussion. J. Geol. 102, 483–485.

Link, P.K., Gostin, V.A., 1981. Facies and paleogeography of Sturtian glacial strata (late Precambrian), South Australia. Am. J. Sci. 281, 353–374.

Martino, R.L., Sanderson, D.D., 1993. Fourier and autocorrelation analysis of estuarine tidal rhythmites, lower Breathitt Formation (Pennsylvanian), eastern Kentucky, USA. J. Sediment. Petrol. 63, 105–119.

McElhinny, M.W., Taylor, S.R., Stevenson, D.J., 1978. Limits to the expansion of the Earth, Moon, Mars and Mercury and to changes in the gravitational constant. Nature 271, 316–321.

McGetchin, T.R., Settle, M., Head, J.W., 1973. Radial thickness variation in impact crater ejecta: implications for lunar basin deposits. Earth Planet. Sci. Lett. 20, 226–236.

Meert, J.G., Van der Voo, R., 1994. The Neoproterozoic (1000–540 Ma) glacial intervals: No more snowball earth? Earth Planet. Sci. Lett. 123, 1–13.

Melosh, H.J., 1989. Impact Cratering. A Geologic Process. Oxford University Press, New York, 245 pp.

Miall, A.D., 1983. Glaciomarine sedimentation in the Gowganda Formation (Huronian), northern Ontario. J. Sediment. Petrol. 53, 477–491.

Munk, W.H., MacDonald, G.J.F., 1960. The Rotation of the Earth. Cambridge University Press, Cambridge, 323 pp.

North, G.R., Cahalan, R.F., Coakley, J.A., 1981. Energy balance climate models. Rev. Geophys. Space Phys. 19, 91–121.
Oberbeck, V.R., Marshall, J.R., Aggarwal, H., 1993. Impacts, tillites, and the breakup of Gondwanaland. J. Geol. 101, 1–19.
Ovenshine, A.T., 1970. Observations of iceberg rafting in Glacier Bay, Alaska, and the identification of ancient ice-rafted deposits. Geol. Soc. Am. Bull. 81, 891–894.
Özsoy, E., 1986. Ebb-tidal jets: a model of suspended sediment and mass transport at tidal inlets. Estuarine Coastal Shelf Sci. 22, 45–62.
Pannella, G., 1976. Geophysical inferences from stromatolite lamination. In: Walter, M.R. (Ed.), Stromatolites. Elsevier, Amsterdam, pp. 673–685.
Park, J.K., 1997. Paleomagnetic evidence for low-latitude glaciation during deposition of the Neoproterozoic Rapitan Group, Mackenzie Mountains, N.W.T., Canada. Can. J. Earth Sci. 34, 34–49.
Peltier, W.R., Jiang, X., 1994. The precession constant of the Earth: Variations through the ice-age. Geophys. Res. Lett. 21, 2299–2302.
Piper, J.D.A., Grant, S., 1989. A palaeomagnetic test of the axial dipole assumption and implications for continental distribution through geological time. Phys. Earth Planet. Inter. 55, 37–53.
Poag, C.W., Aubry, M.-P., 1995. Upper Eocene impactites of the U.S. east coast: depositional origins, biostratigraphic framework, and correlation. Palaios 10, 16–43.
Preiss, W.V. (Compiler), 1987. The Adelaide Geosyncline. Geol. Surv. S. Aust. Bull. 53, 438 pp.
Rosenberg, G.D., Runcorn, S.K. (Eds.), 1975. Growth Rhythms and the History of the Earth's Rotation. Wiley, London, 559 pp.
Rubincam, D.P., 1995. Has climate changed the Earth's tilt? Paleoceanography 10, 365–372.
Runcorn, S.K., 1964. Changes in the Earth's moment of inertia. Nature 204, 823–825.
Runcorn, S.K., 1966. Change in the moment of inertia of the Earth as a result of a growing core. In: Marsden, B.G., Cameron, A.G.W. (Eds.), The Earth–Moon System. Plenum, New York, pp. 82–92.
Runcorn, S.K., 1979. Palaeontological data on the history of the Earth–Moon system. Phys. Earth Planet. Inter. 20, p1–p5.
Schermerhorn, L.J.G., 1974. Late Precambrian mixtites: glacial and/or nonglacial? Am. J. Sci. 274, 673–824.
Schmidt, P.W., Clark, D.A., 1994. Palaeomagnetism and magnetic anisotropy of Proterozoic banded-iron formations and iron ores of the Hamersley Basin, Western Australia. Precambrian Res. 69, 133–155.
Schmidt, P.W., Williams, G.E., 1995. The Neoproterozoic climatic paradox: Equatorial palaeolatitude for Marinoan glaciation near sea level in South Australia. Earth Planet. Sci. Lett. 134, 107–124.
Schmidt, P.W., Williams, G.E., 1996. Palaeomagnetism of the ejecta-bearing Bunyeroo Formation, late Neoproterozoic, Adelaide fold belt, and the age of the Acraman impact. Earth Planet. Sci. Lett. 144, 347–357.
Schmidt, P.W., Williams, G.E., Embleton, B.J.J., 1991. Low palaeolatitude of Late Proterozoic glaciation: early timing of remanence in haematite of the Elatina Formation, South Australia. Earth Planet. Sci. Lett. 105, 355–367.
Scrutton, C.T., 1978. Periodic growth features in fossil organisms and the length of the day and month. In: Brosche, P., Sündermann, J. (Eds.), Tidal Friction and the Earth's Rotation. Springer, Berlin, pp. 154–196.
Sellers, W.D., 1990. The genesis of energy balance modeling and the cool sun paradox. Palaeogeogr., Palaeoclimatol., Palaeoecol. 82, 217–224.
Smith, D.G., Reinson, G.E., Zaitlin, B.A., Rahmani, R.A. (Eds.), 1991. Clastic Tidal Sedimentology. Can. Soc. Pet. Geol. Mem. 16, 387 pp.
Smith, N.D., Phillips, A.C., Powell, R.D., 1990. Tidal drawdown: A mechanism for producing cyclic sediment laminations in glaciomarine deltas. Geology 18, 10–13.
Sonett, C.P., Kvale, E.P., Zakharian, A., Chan, M.A., Demko, T.M., 1996a. Late Proterozoic and Paleozoic tides, retreat of the Moon, and rotation of the Earth. Science 273, 100–104.
Sonett, C.P., Zakharian, A., Kvale, E.P., 1996b. Ancient tides and length of day: correction. Science 274, 1068–1069.
Steiner, M.B., Shoemaker, E.M., 1996. A hypothesized Manson impact tsunami: Paleomagnetic and stratigraphic evidence in the Crow Creek Member, Pierre Shale. Geol. Soc. Am. Spec. Pap. 302, 419–432.
Taylor, S.R., Esat, T.M., 1996. Geochemical constraints on the origin of the Moon. Geophys. Monogr. 95, 33–46.
Toomre, A., 1974. On the 'nearly diurnal wobble' of the Earth. Geophys. J. R. Astron. Soc. 38, 335–348.
Turner, P., 1980. Continental Red Beds. Elsevier, Amsterdam, 562 pp.
Walker, J.C.G., Zahnle, K.J., 1986. Lunar nodal tide and distance to the Moon during the Precambrian. Nature 320, 600–602.
Wallace, M.W., Gostin, V.A., Keays, R.R., 1990. Spherules and shard-like clasts from the late Proterozoic Acraman impact ejecta horizon, South Australia. Meteoritics 25, 161–165.
Wallace, M.W., Gostin, V.A., Keays, R.R., 1996. Sedimentology of the Neoproterozoic Acraman impact-ejecta horizon, South Australia. AGSO J. Aust. Geol. Geophys. 16, 443–451.
Walsh, K.J., Sellers, W.D., 1993. Response of a global climate model to a thirty percent reduction of the solar constant. Global Planet. Change 8, 219–230.
Williams, G.E., 1975. Late Precambrian glacial climate and the Earth's obliquity. Geol. Mag. 112, 441–465.
Williams, G.E., 1979. Sedimentology, stable-isotope geochemistry and palaeoenvironment of dolostones capping late Precambrian glacial sequences in Australia. J. Geol. Soc. Aust. 26, 377–386.
Williams, G.E., 1986a. Precambrian permafrost horizons as indicators of palaeoclimate. Precambrian Res. 32, 233–242.
Williams, G.E., 1986b. The Acraman impact structure: source of ejecta in late Precambrian shales, South Australia. Science 233, 200–203.
Williams, G.E., 1989a. Late Precambrian tidal rhythmites in South Australia and the history of the Earth's rotation. J. Geol. Soc. London 146, 97–111.
Williams, G.E., 1989b. Precambrian tidal sedimentary cycles and

Earth's paleorotation. Eos, Trans. Am. Geophys. Union 70, 33; 40–41.
Williams, G.E., 1989c. Tidal rhythmites: geochronometers for the ancient Earth–Moon system. Episodes 12, 162–171.
Williams, G.E., 1990. Tidal rhythmites: key to the history of the Earth's rotation and the lunar orbit. J. Phys. Earth 38, 475–491.
Williams, G.E., 1991. Upper Proterozoic tidal rhythmites, South Australia: sedimentary features, deposition, and implications for the earth's paleorotation. Can. Soc. Pet. Geol. Mem. 16, 161–177.
Williams, G.E., 1993. History of the Earth's obliquity. Earth-Sci. Rev. 34, 1–45.
Williams, G.E., 1994a. History of Earth's rotation and the Moon's orbit: a key datum from Precambrian tidal strata in Australia. Aust. J. Astron. 5, 135–147.
Williams, G.E., 1994b. Resonances of the fluid core for a tidally decelerating Earth: Cause of increased plume activity and tectonothermal reworking events? Earth Planet. Sci. Lett. 128, 155–167.
Williams, G.E., 1994c. The enigmatic late Proterozoic glacial climate: an Australian perspective. In: Deynoux, M., Miller, J.M.G., Donack, E.W., Eyles, N., Fairchild, I.J., Young, G.M. (Eds.), Earth's Glacial Record. Cambridge University Press, Cambridge, pp. 146–164.
Williams, G.E., 1994d. Acraman: A major impact structure from the Neoproterozoic of Australia. Geol. Soc. Am. Spec. Pap. 293, 209–224.
Williams, G.E., 1996. Soft-sediment deformation structures from the Marinoan glacial succession, Adelaide foldbelt: implications for the palaeolatitude of late Neoproterozoic glaciation. Sediment. Geol. 106, 165–175.
Williams, G.E., 1998. Late Neoproterozoic periglacial aeolian sand sheet, Stuart Shelf, South Australia. Aust. J. Earth Sci., in press.
Williams, G.E., Schmidt, P.W., 1996. Origin and palaeomagnetism of the Mesoproterozoic Gangau tilloid (basal Vindhyan Supergroup), central India. Precambrian Res. 79, 307–325.
Williams, G.E., Schmidt, P.W., 1997. Paleomagnetism of the Paleoproterozoic Gowganda and Lorrain formations, Ontario: low paleolatitude for Huronian glaciation. Earth Planet. Sci. Lett. 153, 157–169.
Witzke, B.J., Anderson, R.R., 1996. Sedimentary-clast breccias of the Manson impact structure. Geol. Soc. Am. Spec. Pap. 302, 115–144.
Young, G.M., 1981. The Early Proterozoic Gowganda Formation, Ontario, Canada. In: Hambrey, M.J., Harland, W.B. (Eds.), Earth's pre-Pleistocene Glacial Record. Cambridge University Press, Cambridge, pp. 807–812.
Young, G.M., 1993. Impacts, tillites, and the breakup of Gondwanaland: a discussion. J. Geol. 101, 675–679.
Young, G.M., Gostin, V.A., 1991. Late Proterozoic (Sturtian) succession of the North Flinders Basin, South Australia; an example of temperate glaciation in an active rift setting. Geol. Soc. Am. Spec. Pap. 261, 207–222.